

# A dual inductor-fed boost converter with an auxiliary transformer and voltage doubler

J. DAWIDZIUK\*

Faculty of Electrical Engineering, Department of Automatic Control Engineering and Electronics, Białystok University of Technology,  
 45D Wiejska St. 15-351 Białystok, Poland

**Abstract.** This paper presents a dual inductor-fed boost converter with an auxiliary transformer and voltage doubler for sustainable energy power converters. The new topology integrates a two-phase boost converter and a dual inductor-fed boost converter. The energy stored and transferred by both inductors can attain a wide input-voltage and load range which uses a constant switching frequency, by controlling the time duration of the simultaneous conduction of the two switches. Among other current-fed type boost converters the presented topology is attractive due to the high voltage conversion ratio, less stress on the components and less switch conduction loss. To verify the feasibility of this topology, the principles of operation, theoretical analysis, and experimental waveforms are presented for a 1 kW prototype.

**Key words:** DC/DC boost converter, current-fed, dual inductor-fed, auxiliary transformer, voltage doubler, photovoltaic systems.

## 1. Introduction

The deepening energy deficit has developed a need to efficiently manage it, especially the noblest kind of energy – electric power. Electrical energy is an undeniable king of energy. Energy saving has become the primary goal of our civilization, because of the depletion of the Earth’s raw materials. Today, the introduction of energy-saving technologies is not a tribute to fashion, but the future of our generation.

The need for huge amounts of clean and renewable energy is the reason, that photovoltaic energy has recently been fully appreciated since it reduces greenhouse gas emissions and ensures the availability of energy in the future. Solar energy can be utilized as heat power or as electrical power by means of photovoltaic conversion. Solar energy produced during the photovoltaic conversion can be utilized as heat power or electrical power.

In many renewable energy applications high efficiency, high power, and high voltage boost DC/DC converters are required as an integral interface between the available low voltage sources and the output loads which operate at higher voltages. Examples of recent applications are photovoltaic systems that require high-gain dc voltage conversion. In these applications non-isolated boost DC/DC converters can be used, but they should operate at high efficiency while conducting high currents from low-voltage dc sources at their inputs. Low input voltage results in large currents flowing through the switches. High  $R_{on}$  resistance of the switches increases conduction losses and the reverse recovery problem can reduce efficiency. Moreover, parasitic components cause additional voltage overshoots creating the need to use switches with higher blocking voltages, which further increases losses. These voltage spikes are not only dangerous to the switches but they substantially increase the switching losses.

Converters with high frequency transformers have been commonly used for many years. However, when there is no need to use galvanic isolation between the input and the output, non-isolated boost DC/DC converters are the recommended solution [1–3].

The dual-inductor boost converter exhibits benefits in high power applications: high input current is split between two inductors, thus reducing  $I^2R$  power loss in both copper windings and primary switches.

## 2. Operational principle

A dual inductor-fed boost converter with an auxiliary transformer and voltage doubler is shown in Fig. 1 [4]. In order to explain the principles of its operation, the converter is analyzed in steady-state and continuous conduction mode, with switches’ duty cycle above 50%.

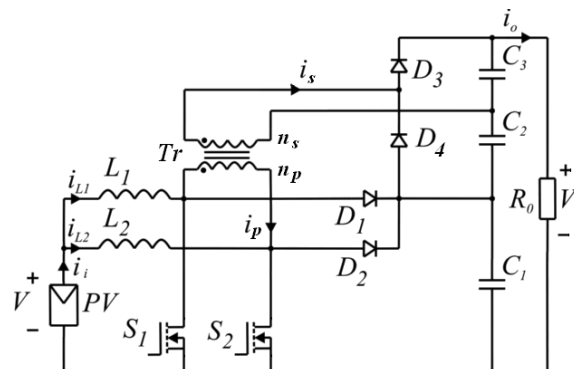


Fig. 1. A non-isolated dual inductor-fed boost converter with an auxiliary transformer and voltage doubler ( $n = n_s/n_p$ ): dual inductor-fed boost converter – ( $V_i, L_1, L_2, S_1, S_2, Tr, D_3, D_4, C_2, C_3$ ); two-phase boost converter – ( $V_i, L_1, L_2, S_1, S_2, D_1, D_2, C_1$ )

\*e-mail: j.dawidziuk@pb.edu.pl

Key waveforms are shown in Fig. 2. The circuit's operation can be divided into four stages or intervals, which are described as follows:

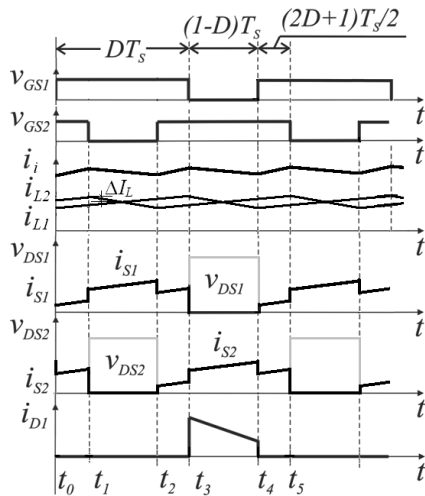


Fig. 2. Theoretical waveforms of the converter with  $D > 0.5$

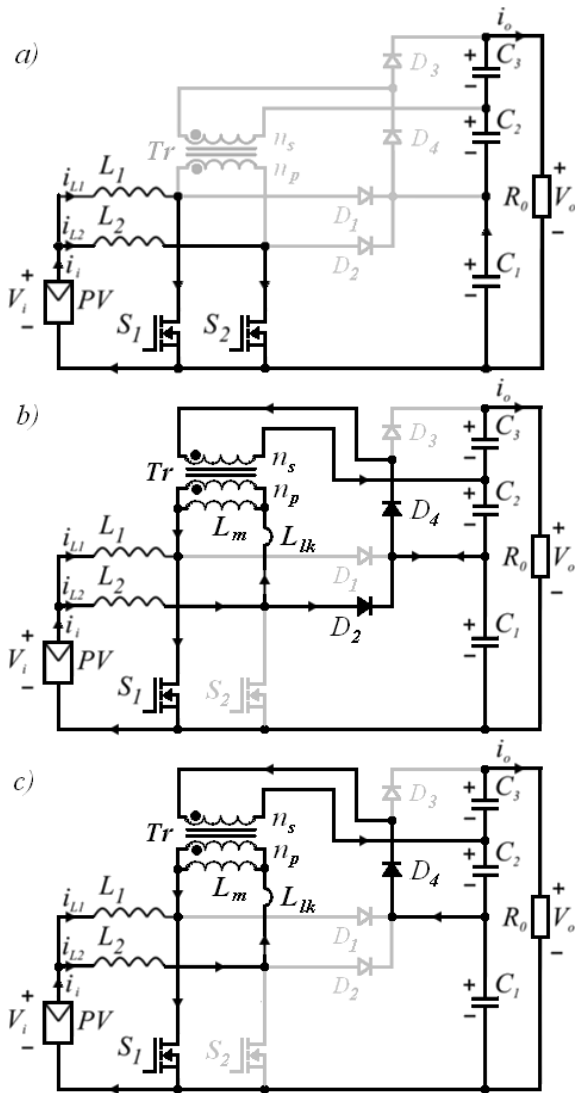


Fig. 3. Operation stages of the converter

*Stage 1* ( $t - t_1$ ). Switches  $S_1$  and  $S_2$  are conducting (Fig. 3a). The input current increases linearly and energy is stored in inductors  $L_1$  and  $L_2$ . The primary winding  $n_p$  is shorted and does not induce voltage in the secondary winding  $n_s$ . The diodes  $D_1 - D_4$  are reverse biased, and the load is supplied from capacitors  $C_1 - C_3$ .

*Stage 2* ( $t_1 - t_2$ ). The switch  $S_2$  is turned-off at time  $t_1$  (Fig. 3b). Inductance current  $i_{L2}$  through the diode  $D_2$  charges the capacitor  $C_1$ , and through the transformer and the diode  $D_4$  capacitor  $C_2$  (if the voltage across the secondary winding of the transformer is larger than the capacitor voltage  $v_{C2}$ ). After turning  $S_2$  off and turning  $D_2$  on, the voltage across  $S_2$  is limited to  $v_{C1}$ , thus additional dissipative clamping circuits are not required. If, before  $S_2$  switch is turned-on diode  $D_2$  will be turned-off, an additional state shown in Fig. 3c occurs.

*Stage 3* ( $t_2 - t_3$ ). Stage 3 is the same as stage 1.

*Stage 4* ( $t_3 - t_4$ ). Switch  $S_1$  is turned-off and  $S_2$  remains on. Diodes  $D_1$  and  $D_3$  conduct and capacitors  $C_1$  and  $C_3$  are recharged during stage 4.

Since the output capacitors are connected in a series the average currents into each output capacitor are the same at the steady state regardless of the duty ratio. The average forward current of diodes  $D_1$  and  $D_2$  equals half of the output DC current, because these diodes are connected in parallel. The average forward current of diodes  $D_3$  and  $D_4$  is equal to the output DC current  $I_O$ .

### 3. Steady-state analysis

A dual inductor-fed boost converter with an auxiliary transformer and voltage doubler integrates two inverters: a dual inductor-fed boost converter and a two-phase boost converter. This topology has similar features to a non-isolated push-pull boost converter [3].

The two-phase boost converter operates in the same way as the basic boost converter, voltage gain  $B_1$  does not change and it is stated as

$$B_1 = \frac{V_o}{V_i} = \frac{V_{C1}}{V_i} = \frac{1}{1 - D}, \quad (1)$$

where  $V_o$  is the output voltage,  $V_i$  is the input voltage,  $V_{C1}$  is the voltage across the capacitor  $C_1$ , and  $D$  is the duty cycle.

The capacitor voltage  $v_{C1}$  is being applied to the primary winding  $n_p$  and voltage  $n \cdot v_{C1}$  induces in the secondary winding  $n_s$ . This bipolar voltage charges capacitors  $C_2$  and  $C_3$  to double the voltage across the secondary winding.

Voltage gain  $B_2$  of the dual inductor-fed with a voltage doubler boost converter is equal to

$$B_2 = \frac{V_{C34}}{V_i} = \frac{2nV_{C1}}{V_i} = \frac{2n}{1 - D}. \quad (2)$$

In (2),  $V_{C34}$  is the voltage across the capacitors  $C_2$  and  $C_3$ , and  $n = n_s/n_p$  is the transformer turn ratio.

The proposed converter is a series-output scheme satisfying

$$V_o = V_{C1} + V_{C2} + V_{C3}. \quad (3)$$

### A dual inductor-fed boost converter with an auxiliary transformer and voltage doubler

After taking into account the relations mentioned above, the voltage gain of the dual inductor-fed boost converter with voltage doubler is given as

$$B = \frac{1 + 2n}{1 - D}. \quad (4)$$

The operating voltage switches  $S_1$ ,  $S_2$ , diodes  $D_1 - D_4$  and capacitors  $C_1 - C_3$  describe the following relationships:

$$V_{S1(off)} = V_{S2(off)} = V_{D1(R)} = V_{D2(R)} = V_{C1} = \frac{V_o}{1 + 2n} = \frac{V_i}{1 - D}, \quad (5)$$

$$V_{D3(R)} = V_{D4(R)} = \frac{2nV_o}{1 + 2n} = \frac{2nV_i}{1 - D}, \quad (6)$$

$$V_{C2} = V_{C3} = \frac{nV_o}{1 + 2n} = \frac{nV_i}{1 - D}. \quad (7)$$

Taking into account the boundary conditions for the equation  $i_{L1} = I_{L1 \min} + (V_i/L_1)t$ , describing the current inductor  $L_1$  between  $t_0 - t_1$ , the current ripple on the inductor is equal to

$$\Delta I_{L1} = \frac{V_o(1 - D)(2D - 1)}{2f_s L_1(1 + 2n)}, \quad (8)$$

where  $f_s$  is the switching frequency of the converter.

From

$$\bar{\Delta I}_{L1} = (1 - D)(2D - 1) = (2f_s L_1 \Delta I_{L1} (2n + 1))/V_o$$

sets the maximum value  $\bar{\Delta I}_{Lb} = 0.125$  for  $D = 0.75$ . In this way, for a certain value to the current ripple, it is possible to calculate the inductor value using

$$L_1 = \frac{V_o}{16f_s \Delta I_{L1} (1 + 2n)}. \quad (9)$$

The capacity of each capacitor can be estimated using the expressions

$$C_1 \geq \frac{DT_s V_o}{2R_o \Delta V_o} = \frac{D(1 - D)P_o}{2f_s(1 + 2n)V_i \Delta V_o}, \quad (10)$$

$$C_2 = C_3 \geq \frac{D(1 - D)P_o}{f_s(1 + 2n)V_i \Delta V_o}. \quad (11)$$

In (10) and (11),  $P_o$  is the converter output power, and  $\Delta V_o$  is half the peak to peak output voltage ripple.

Total conduction losses in the primary switches of the dual inductor-fed boost converter with a voltage doubler are expressed as

$$P_{Scon} = R_{on} \left[ (1 - D) \left( \frac{1}{2} + \frac{n}{1 + 2n} \right)^2 + \frac{2D - 1}{4} \right] \left( \frac{P_o}{V_i} \right)^2. \quad (12)$$

In the presented circuit the two-phase boost converter plays a crucial role to improve total efficiency. If snubber circuits only suppress voltage across the switch, surge energy is dissipated as heat. On the contrary, in the two-phase boost converter the surge energy can be transmitted to the load.

## 4. Experimental results

In order to verify the operation principle of the proposed converter and the design methods analyzed theoretically above, a laboratory prototype has been assembled and tested. The specifications and parameters of the converter are given in Table 1.

Table 1  
Main specifications and components of the prototype

Description	Values
Input voltage	(9-31) VDC
Output voltage	(110-380) VDC
Switching frequency	48 kHz
Switches $S_1$ and $S_2$	IRFP4668PBF(200 V/130A/8mΩ)
Diodes $D_1 - D_4$	C2D20120D (1200 V/20 A/1.6 V)
Capacitor $C_1$	10 μF/350 V MKP VISHAY
Capacitors $C_2 - C_3$	470 μF/400 V electrolytic
Inductors $L_1 = L_2$	DTMSS-47/0.068/45, 20 turns
Transformer $Tr$	Payton Planar P.N.56960/1000DC-8-16, $n=2$
Photovoltaic generator	10 PV module KD320GH-4YB
PV array	in parallel: 3.2 kW at 1000 W/m <sup>2</sup>

The assumed parameters are: the maximum boost inductor current ripple  $\Delta I_L = 0.2I_{iL \max}$ , the maximum duty cycle of the switches  $D_{\max} = 0.70$  to minimum input voltage, and the output voltage ripple  $\Delta V_o = 0.01V_o$ .

The efficiency of the converter was measured with a Power Analyzer 3390-Hioki, and the results were verified with digital devices and conventional meters by making measurements of input and output voltages and currents.

Figures 4–8 shows the experimental waveforms of the dual inductor-fed boost converter with an auxiliary transformer and voltage doubler at the main operation region.

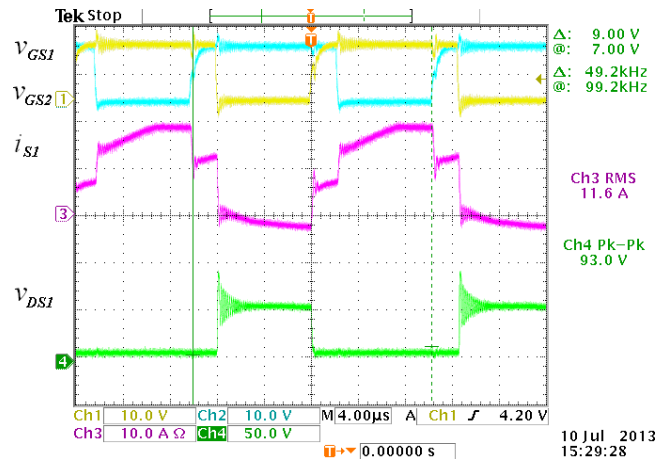


Fig. 4. Gate-to-source voltages  $v_{GS1}$  and  $v_{GS2}$ , drain current  $i_{S1}$  and drain-to-source voltage  $v_{DS1}$

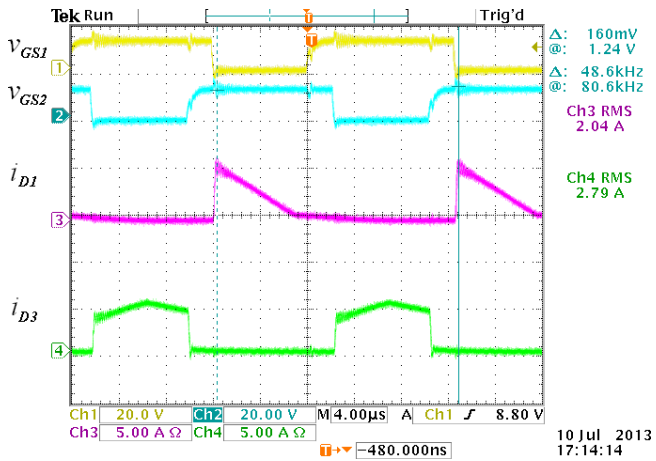


Fig. 5. Gate-to-source voltages  $v_{GS1}$  and  $v_{GS2}$ , current through diodes  $i_{D1}$  and  $i_{D3}$

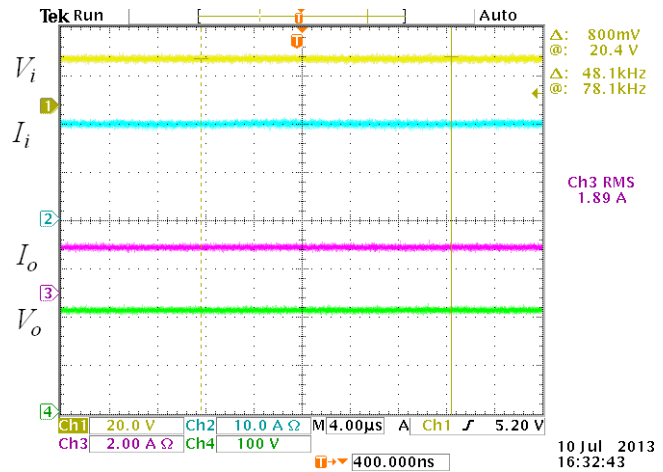


Fig. 8. Input voltage  $V_i$ , input current  $I_i$ , output current  $I_o$  and output voltage  $V_o$

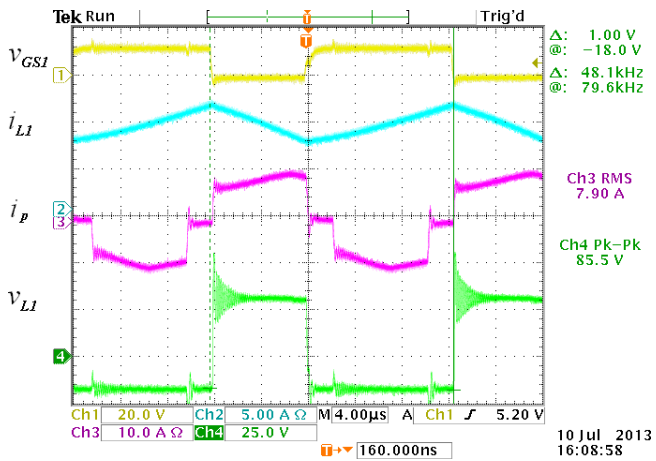


Fig. 6. Gate-to-source voltage  $v_{GS1}$ , current through the inductor  $i_{L1}$ , primary current through the transformer  $i_p$  and voltage across the inductor  $v_{L1}$

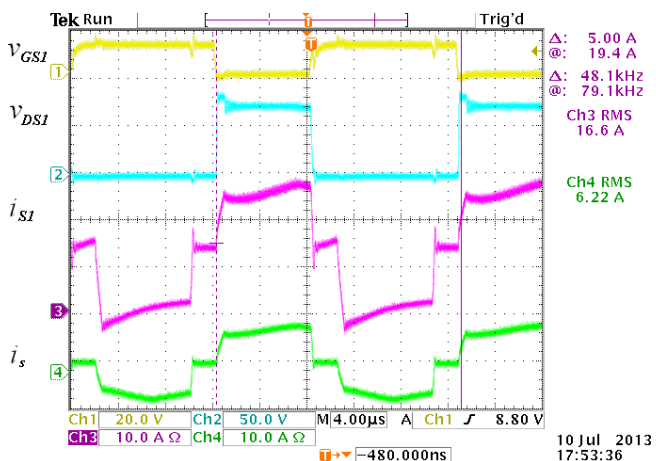


Fig. 7. Gate-to-source voltage  $v_{GS1}$ , drain-to-source voltage  $v_{DS1}$ , drain current  $i_{S1}$  and secondary current through the transformer  $i_s$  ( $V_i = 31$  V,  $I_i = 37$  A,  $v_{DS1max} = 95$  V,  $V_o = 373$  V,  $D = 0.6$ ,  $B = 12$ )

Taking into account waveforms of switches' voltage (e.g.  $v_{DS1}$  in Fig. 7), it is possible to show, that the converter has properties of self-clamping of the voltage (the snubber circuit is not needed). When the switches are turning off, the parallel boost diodes ( $D_1$ ,  $D_2$ ) and output capacitor ( $C_1$ ) act as a voltage clamping circuit. According to Fig. 7, the drain-to-source voltage in  $S_1$  is lower than one fifth output voltage, as expected in the theoretical analysis. The voltage level across the switch  $S_1$  is reduced to the voltage level on the capacitor  $C_1$ .

The duty ratio is about 0.6 (theoretically 0.58) to satisfy output voltage level at main operation region as shown in Fig. 7 and Fig. 8.

The two-phase boost converter in the proposed scheme performs the surge energy to be clamped, surge energy is transmitted to the load (Fig. 7), thus increasing the efficiency of the converter.

Figure 9 shows the efficiency of the converter within the range between (100–1000) W of output power, at the switching frequency  $f_s = 48$  kHz and the duty cycle  $D = 0.6$ . The measurements show efficiency of 91.7% at full load conditions, the efficiency is 94.3% near the half load conditions and the maximum efficiency reached 95.7% at 100 W of output power. The proposed converter has a flatter and higher

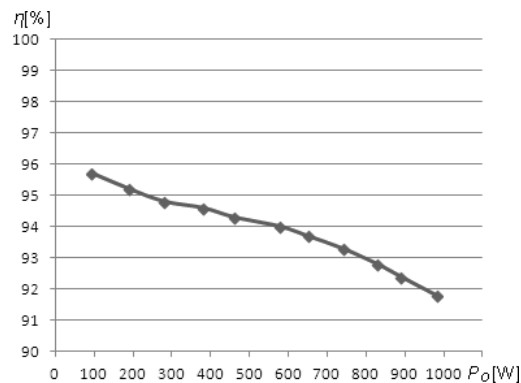


Fig. 9. Measured converter efficiency (3390-Hioki-accuracy  $\pm 0.16\%$  with current sensors), as a function of the output power,  $D = 0.6$

## A dual inductor-fed boost converter with an auxiliary transformer and voltage doubler

efficiency curve rather than the conventional circuits in wide load ranges. This high efficiency is strongly resulted from the versatile two-phase boost converter.

A comparison of the efficiency current-fed dual-inductor boost converters is listed in Table 2 [5–10].

Table 2  
A comparison of efficiency

Converter References	Input Voltage [V]	Voltage Gain [V/V]	Output Power [W]	Maximum Efficiency [ $\eta$ %]
[5]	40	9.5	1000	92.0
[6]	42	9.5	200	95.3
[7]	34	8.3	600	95.4
[8]	70	7.6	1900	88.9
[9]	30	12.6	100	92.4
[10]	40	10	400	91.7
proposed	30	12	100/1000	95.7/91.7

The comparison shows that among other current-fed type boost converters the topology presented is attractive due to the highest voltage conversion ratio and efficiency.

A preliminary test of the converter powered by a photovoltaic generator with a power output of 3.2 kW has been carried out.

## 5. Conclusions

The converter described is suitable for applications that require a very high input-to-output voltage conversion ratio. Specifically, non-isolated implementation with an auxiliary transformer ( $n = 2$ ) and a voltage-doubler rectifier exhibits a voltage gain that is five times higher than that of the corresponding gain of a conventional non-isolated boost converter, and more than 1.5 times higher when compared to a non-isolated push-pull-boost converter. Serial connection of all capacitors improves the voltage gain. The examined non-isolated DC/DC converter can operate with a high voltage gain  $B > 10$ , same as transformer isolated converters, without the need to work at extreme values of duty cycle  $D < 0.6$ . This topology utilizes a simple two-winding transformer, reduces voltage stress on the switches and smoothes out the input current.

The main drawbacks of this topology are the several diodes connected in series and the three serial connected output capacitors. Moreover, the voltage overshoots caused by

parasitic parameters are present in the practical circuit. It induces additional voltage stresses and necessitates the use of switches with a higher blocking voltage, which leads to more losses and reduced efficiency.

Despite the drawbacks mentioned this topology is a good solution to photovoltaic systems.

**Acknowledgements.** This work was supported by the Polish National Science Centre as a research project NN510 5120 40.

## REFERENCES

- [1] P. Zacharias, B. Sahan, S.V. Araujo, F.L.M. Antunes, and R.T. Bascope, "Analysis and proposition of a pv module integrated converter with high voltage gain capability in a non-isolated topology", *7<sup>th</sup> Int. Conf. on Power Electronics 1*, CD-ROM (2007).
- [2] P. Klimczak and S. Munk-Nielsen, "High efficiency boost converter with three state switching cell", *Int. Exhibition & Conf. Power Electronics, Intelligent Motion, Power Quality PCIM Eur. 1*, 143–148 (2009).
- [3] J. Dawidziuk, "A current-fed push-pull dc/dc boost converter for coupling PV modules with PWM voltage-source inverter", *Electrical Review* 89, 15–18 (2013).
- [4] P. Klimczak, "Modular power electronic converters in the power range 1 to 10 kW", *PhD Thesis*, Institute of Energy Technology, Aalborg, 2009.
- [5] Y. Jang and M.M. Jovanovic, "New two-inductor boost converter with auxiliary transformer", *Applied Power Electronics Conf. 1*, 654–660 (2002).
- [6] H. Seong, K. Park, G. Moon, and M.J. Youn, "Novel dual inductor-fed dc/dc converter integrated with parallel boost converter", *39th IEEE Power Electronics Specialists Conf. 1*, 2125–2131 (2008).
- [7] C.S. Leu and M.H. Li, "A novel current-fed dual-inductor boost converter with current ripple reduction (DIBCRR) for high output-voltage applications", *Energy Conversion Congress and Exposition. ECCE 2009, IEEE 1*, 2191–2197 (2009).
- [8] G. Kishor, D. Subbarayudu, and S. Sivanagaraju, "Comparison of full bridge and two inductor boost converter systems", *J. Theoretical and Applied Information Technology* 34, 118–124 (2011).
- [9] K.J. Lee, B.G. Park, R.Y. Kim, and D.S. Hyun, "Nonisolated ZVT two-inductor boost converter with a single resonant inductor for high step-up applications", *IEEE Trans. Power Electronics* 27, 1966–1973 (2012).
- [10] A. Tomaszuk and A. Krupa, "Step-up DC/DC converters for photovoltaic applications – theory and performance", *Electrical Review*. 89, 51–57 (2013).